Muon-Proton Elastic Scattering at High Momentum Transfers*

R. W. ELLSWORTH,† A. C. MELISSINOS, J. H. TINLOT,‡ H. VON BRIESEN, JR.,§ AND T. YAMANOUCHI
Department of Physics and Astronomy, The University of Rochester, Rochester, New York

AND

L. M. LEDERMAN AND M. J. TANNENBAUM‖
Nevis Laboratories, Columbia University, New York, New York

AND

R. L. COOL AND A. MASCHKE
Brookhaven National Laboratory, Upton, New York

(Received 25 July 1967)

We have measured the muon-proton elastic scattering cross section $d\sigma/dq^2$ for momentum transfers in the range $10\ \mathrm{F}^{-2} < q^2 < 31\ \mathrm{F}^{-2}$ using a broad-spectrum muon beam of momenta between 1.5 and 6.0 BeV/c. The muons were incident upon a large hydrogen target surrounded by an array of spark chambers and scintillation counters. We have compared our results with the equivalent electron-proton cross section to obtain a limit on the electromagnetic muon-electron difference. Assuming a lepton-vertex form factor of the type $f(q^2)=(1+q^2/\Lambda^2)^{-1}$, and defining the muon-electron difference parameter D^2 by $1/D^2=1/\Lambda_\mu^2-1/\Lambda_e^2$, we find for the 95% confidence limit $D^2 \geq 107\ \mathrm{F}^{-2}$ ($D^{-1} \leq 0.09$ F; $D \geq 2.04$ BeV/c).

I. INTRODUCTION

THE muon has been a much studied particle in the 35 years since its discovery. In the past 20 years, there has been a growing awareness of its resemblance to the electron in its weak, electromagnetic, and (absence of) strong interactions. Paralleling this, there is recently great success in the notion that particle families derive from a common mass level, split by interactions which lift the degeneracy arising from some natural symmetry. This then has sharpened the dilemma of why the muon and electron should have so large a mass difference in spite of the detailed and quantitative identity of interactions so far observed.[1]

The basis of this research is the notion that comparison of muon and electron scattering from protons at ever increasing values of the momentum transfer will decide whether or not the identity of electromagnetic structure of these two particles persists down to very small distances, or alternatively whether small traces can be uncovered, in the electromagnetic structure, of some heretofore unknown interaction. Preliminary results previously reported[2] did not include data at low momentum transfer which are included here, together with fuller details on the experimental technique, especially its unique off-line features.

Muon scattering from complex nuclei has been measured at low momentum transfer.[3–5] The only previous muon-proton experiment was carried out at the Bevatron[6] in the momentum transfer region $6 < q^2 \leq 18\ \mathrm{F}^{-2}$. The present experiment utilized a highly purified, wide-momentum-band muon beam and yielded ~1000 events in the interval of momentum transfer from $10 \leq q^2 \leq 31\ \mathrm{F}^{-2}$. A summary of muon elastic scattering results is given in Table I(a).

Electromagnetic differences between the muon and the electron can be tested for in different types of experiments, for example: measurement of the anomalous magnetic moment,[7] lepton pair photoproduction,[8,9] and lepton-lepton scattering.[10,11] In Table I(b) we summarize some of these results.

The muon-proton scattering cross section is given by

* Work supported in part by the U. S. Atomic Energy Commission, Contracts No. AT(30-1)-875, University of Rochester, and No. AT(30-1)-1932, Columbia University.

† Present address: University of Washington, Seattle, Wash.

‡ Deceased.

§ Present address: Northeastern University, Boston, Mass.

‖ Present address: Harvard University, Cambridge, Mass.

[1] G. Feinberg and L. Lederman, Ann. Rev. Nucl. Sci. **13**, 431 (1963).

[2] R. Cool, A. Maschke, L. M. Lederman, M. Tannenbaum, R. Ellsworth, A. Melissinos, J. H. Tinlot, and T. Yamanouchi, Phys. Rev. Letters **14**, 724 (1965).

[3] P. L. Connolly, J. G. McEwen, and J. Orear, Phys. Rev. Letters **6**, 554 (1961).

[4] A. Citron, C. DeLorme, D. Fries, L. Goldzahl, J. Heintze, E. G. Michaelis, C. Richard, and H. Øveras, Phys. Letters **1**, 175 (1962).

[5] G. E. Masek, L. D. Heggie, Y. B. Kim, and R. W. Williams, Phys. Rev. **122**, 937 (1961); C. Y. Kim, S. Kaneko, Y. B. Kim, G. E. Masek, and R. W. Williams, *ibid.* **122**, 1641 (1961).

[6] H. F. Davis, T. E. Ewart, G. E. Masek, E. D. Platner, J. P. Toutonghi, and R. W. Williams, Phys. Rev. **131**, 2192 (1963).

[7] G. Charpak, F. J. M. Farley, R. L. Garwin, T. Muller, J. C. Sens, and A. Zichichi, Nuovo Cimento **37**, 1241 (1965); also F. M. J. Farley, J. Bailey, R. C. Brown, M. Giesch, H. Jolstein, J. Van der Meer, E. Picasso, and M. J. Tannenbaum, *ibid.* **45A**, 281 (1966). $(g-2)/2=(1165\pm3)\times10^{-6}$ for μ^- and $(g-2)/2=(1162\pm5)\times10^{-6}$ for μ^+.

[8] J. K. de Pagter, J. I. Friedman, G. Glass, R. C. Chase, M. Gettner, E. VonGoeler, R. Weinstein, and A. M. Boyarski, Phys. Rev. Letters **17**, 767 (1966).

[9] J. G. Asbury, W. K. Bertram, U. Becker, P. Joos, M. Rohde, A. J. S. Smith, S. Friedlander, C. L. Jordan, and C. C. Ting, Phys. Rev. Letters **18**, 65 (1967). For the parametrization of the photoproduction experiments see, however, N. M. Kroll, Ref. 41 of this paper.

[10] W. C. Barber, B. Gittelman, G. K. O'Neill, and B. Richter, Phys. Rev. Letters **16**, 1127 (1966).

[11] G. Backenstoss, B. D. Hyams, G. Knop, P. C. Marin, and U. Stierlin, Phys. Rev. **129**, 2759 (1963).

TABLE I. Comparison of experiments probing the electromagnetic structure of muons and electrons.

(a) Results from muon scattering experiments.[a]

Experiment	Target	Incident momentum or energy	Flux	Momentum transfer (MeV/c)	(95% confidence level) D^2 (F^{-2})	D (BeV/c)
Connolly *et al.* (1961, Ref. 3)	Emulsions	43-MeV μ^+		80–160	2	0.28
Masek *et al.* (1961, Ref. 5)	Carbon, lead	2.0 BeV/c	2.5×10^7	70–400	4	0.41
Citron *et al.* (1962, Ref. 4)	Carbon	180, 240 MeV/c		76–250	11	0.71
Davis *et al.* (1963, Ref. 6)	Liquid hydrogen	1.21 BeV/c	3×10^8	450–850	36	1.2
This experiment	Liquid hydrogen	1.5–6 BeV/c		630–1100	107	2.04

(b) Results from related experiments.[b]

Experiment	Momentum transfer	Vertex breakdown parameter (95% confidence level)	
Charpak *et al.* (1965, Ref. 7)	$g-2$ for μ^+	$\Lambda_\mu^2\geq31$ F^{-2}	$\Lambda_\mu\geq1.1$ BeV/c
Barber *et al.* (1966, Ref. 10)	e-e scattering 200–400 MeV/c	$\Lambda_e^2\geq15$ F^{-2}	$\Lambda_e\geq0.76$ BeV/c
Backenstoss *et al.* (1963, Ref. 11)	μ-e scattering $1/\Lambda^2=1/\Lambda_e^2+1/\Lambda_\mu^2$	$\Lambda^2\geq$ 2.4 F^{-2}	$\Lambda\geq0.30$ BeV/c
de Pagter *et al.* (1964, Ref. 8)	μ-pair photoproduction $q^2<400$ (MeV/c)^2		
Asbury *et al.* (1966, Ref. 9)	e-pair photoproduction $q^2<400$ (MeV/c)^2		

[a] D is the difference parameter defined in the text, Eq. (3), and D^{-1} is approximately the interaction distance within which the equality of electron-muon structure has been probed.
[b] Here Λ^{-1} is the "vertex breakdown distance" introduced by Drell (see Ref. 38). The parametrization of the photoproduction experiments is not given directly in terms of the vertex (see Refs. 40 and 41).

the Rosenbluth formula,[12] written here in invariant form:

$$\frac{d\sigma}{dq^2}=\frac{4\pi\alpha^2}{q^4}\frac{G^2(q^2)}{1+q^2/4M^2}\left[1-\frac{q^2}{2ME}+\frac{q^2}{4E^2}\left(\frac{q^2}{2M^2}\frac{1+q^2/4M^2}{q^2/4M^2+G_E^2/G_M^2}-1\right)\right], \quad (1)$$

where $G^2(q^2)$ is a combination of the electric and magnetic form factors

$$G^2(q^2)=G_E^2(q^2)+(q^2/4M^2)G_M^2(q^2). \quad (2)$$

$\alpha=e^2/\hbar c$ is the fine-structure constant, M the mass of the proton, E the laboratory energy of the incident lepton, and q^2 is the square of the four-momentum transferred to the proton.[13] In Eq. (1) the mass of the lepton has been neglected. Any structure effects of the leptons are assumed to manifest themselves in a single form factor[14] $f(q^2)$ which can be considered as already included in $G^2(q^2)$.

[12] M. N. Rosenbluth, Phys. Rev. **79**, 615 (1950). We set $\hbar=c=1$.
[13] We choose q^2 positive in the spacelike region.
[14] K. J. Barnes, Nuovo Cimento **27**, 229 (1963); A. I. Nikishov, Zh. Eksperim. i Teor. Fiz. **36**, 1604 (1959) [English transl.: Soviet Phys.—JETP **9**, 1140 (1959)].

In the region of this experiment the energy dependence of $d\sigma/dq^2$ is weak. This permitted us to obtain scattering data with a broad-momentum-band muon beam, but did not allow us to deduce the separate contributions from $G_M(q^2)$ and $G_E(q^2)$.

II. EXPERIMENT: GENERAL CONSIDERATIONS

In performing a measurement of μ-p elastic scattering there are certain general features which imposed special constraints on the design of the experiment. We would like to briefly mention these factors before entering into a more detailed description of our experimental setup.

(1) At a proton accelerator, such as the AGS, a muon beam must be obtained from the decay in flight of pions; therefore the phase-space characteristics and intensity are in general inferior to those of pion or kaon beams. The smallness of the μ-p cross section made it advantageous to use a broad band of momenta in the incident beam. The beam achieved had a momentum band from 1 to 6 BeV/c and a flux at the target of 2×10^6 muons per AGS pulse of $\sim2\times10^{11}$ protons.

(2) The μ-p elastic cross section is smaller than the corresponding π-p cross section[15] by a factor of $\gtrsim10^4$

[15] M. L. Perl, L. W. Jones, and C. C. Ting, Phys. Rev. **132**, 1252 (1963).

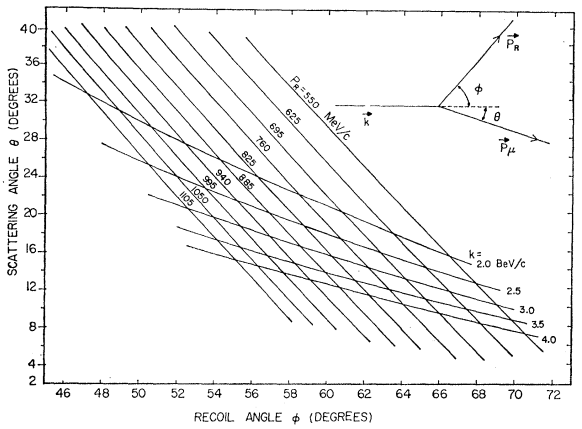

FIG. 1. Kinematic relation between the scattering angle θ, the recoil angle φ, and the incident muon momentum k, and the recoil proton momentum P_R.

necessitating a very high effective beam purity (10^6 μ's per π for 1% contamination). Assuming the π/μ ratio in the beam to be $\sim$10, one requires pion rejection by a factor of the order of 10^7 to 10^8. Such rejection was achieved by passing the beam through a large amount of absorber. A limitation in this technique arises from the electroproduction of pions by the muon flux in the absorber; we estimate this process to occur at the level of $\sim 10^{-6}$, a more detailed discussion being given in Appendices I and II.

(3) Next we consider the geometry of the experiment. In principle, for elastic scattering, if the incident direction and energy are known, measurement of one parameter (the scattering angle θ or q^2) is sufficient; in addition one needs to overconstrain the event to establish that the scattering is elastic. In the present experiment, since the incoming energy was not known, we chose to measure the proton and muon scattering angles as well as the energy of the recoil proton. Furthermore, the laboratory kinetic energy T of the proton is directly related to the momentum transfer for elastic events ($q^2=2MT$). The lower limit on q^2 was imposed by the requirement that the recoil protons have sufficient energy to leave the hydrogen target and be detected in the apparatus. In Fig. 1 are given the kinematic relations between θ, φ, P_R, and k, where k is the incident momentum and φ, P_R are the proton recoil angle and momentum, respectively.

In view of the small cross section and of the limited flux, a long H_2 target and a large-solid-angle detector were desirable. Two large spark chambers were used to measure the proton angle and range, and separate spark chambers detected the scattered muon. A schematic of the beam is shown in Figs. 2(a) and (b) and of the apparatus in Figs. 3(a) and (b).

(4) We wish to comment on the recoil proton energy determination by range in the region of $200<T<650$ MeV as used in our experiment. The probability for nuclear interaction of a proton before it reaches the end of its range is significant especially at the higher momenta; see Fig. 4. Thus only a fraction of the elastically scattered recoil protons will fulfill the kinematical criteria for elastic scattering. The elastic scattering cross section can be determined if the probability for loss due to nuclear interaction is known. Since the nuclear interaction involves elastic proton-aluminum as well as complex events, this was studied experimentally in an ancillary run. The results were taken into account by using a Monte Carlo program. This is discussed in Appendix III.

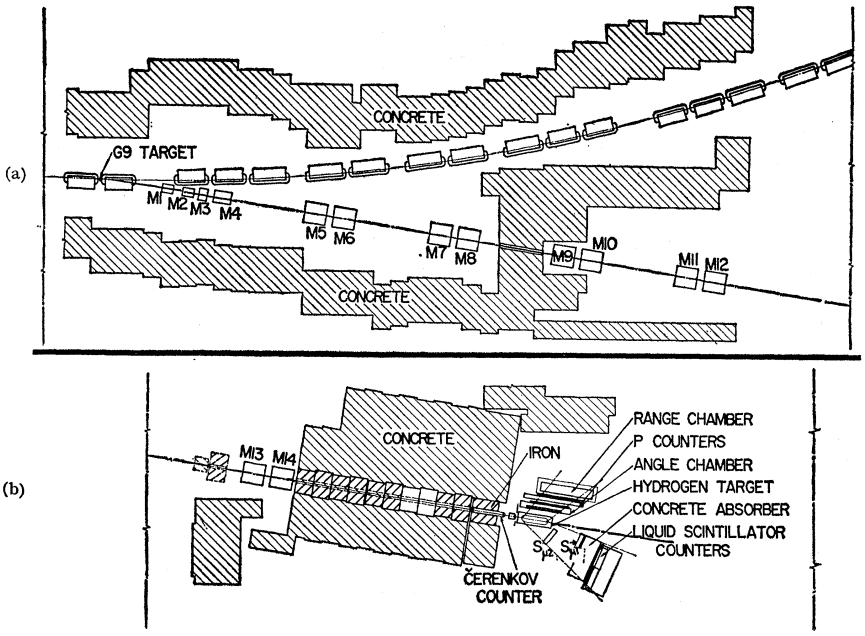

FIG. 2. The muon beam layout. Pions produced at $\sim$0° at the G-9 target were deflected outward by the G-10 magnet of the AGS. The quadrupole channel collected and held pions of energy 6–10 BeV. The first four magnets were run as a single strong-focusing triplet lens. The remainder were operated as strong-focusing doublet lenses.

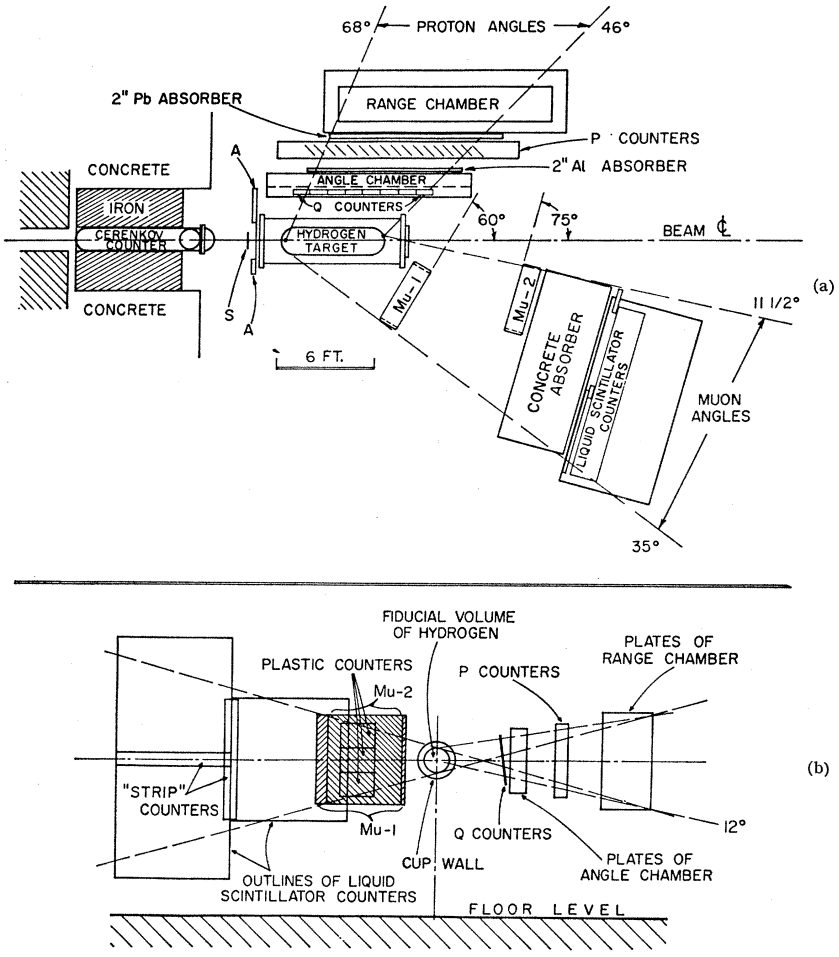

FIG. 3. Experimental layout. (a) Runs B and C, top view. The 2-in. lead absorber was removed for run B. (b) Runs B and C, axial projection. For run A, the 3 large plastic counters were absent, and all components were moved closer toward the beam.

III. EXPERIMENTAL LAYOUT: DETAILS

A. Muon Beam

As mentioned previously, muons were obtained from the decay of negative pions in the magnetic transport system shown in Fig. 2. In order to increase the flux, the internal AGS target was located at the G-9 position, so that negative pions with production angles close to 0° could be collected by the transport system.

The first four quadrupoles shown in Fig. 2 were of 8-in. aperture to permit close placement to the AGS ring and were run as a quadrupole triplet. The remainder were run as a sequence of quadrupole doublets. The beam was designed to give maximum muon flux in the momentum band of interest with the available number of quadrupoles. Pions of 6–10-BeV energies were collected and held by the transport system for a distance of 183 ft, in which length about 12% of them could decay. We estimate that for 10^{11} internal protons in the AGS, approximately 10^7 muons of energy greater than 6 BeV were produced and trapped in the transport system.

To obtain the desired high purity of muons the beam was passed through 32 ft of light concrete (see Fig. 2). As discussed in Appendix I, this corresponds to 19 pion absorption lengths which results in an attenuation of pions by a factor larger than 10^8. The actual limit, however, on the attainable beam purity arises from the electroproduction of pions by muons passing through the filter; such pions are of low energy and have been estimated not to exceed 10^{-6} of the muon beam (see Appendix II).

An additional absorber of 4 ft of heavy concrete (see Fig. 3) was placed just in front of the muon trigger counters. The purpose of this absorber was manifold:

(1) By range it set a limit on the energy of the scattered muon such that $E_\mu > 0.8$ BeV.

(2) It eliminated background from electron-proton scattering.[16]

(3) It attenuated any strongly interacting particles by a factor of ~12 and therefore suppressed the background from scattering of regenerated pions.

The effectiveness of these filtering arrangements was measured by observing the apparent increase in the

[16] A small fraction of the beam (few percent) contained electrons which were knock-ons produced by the muons in the last sections of the filter.

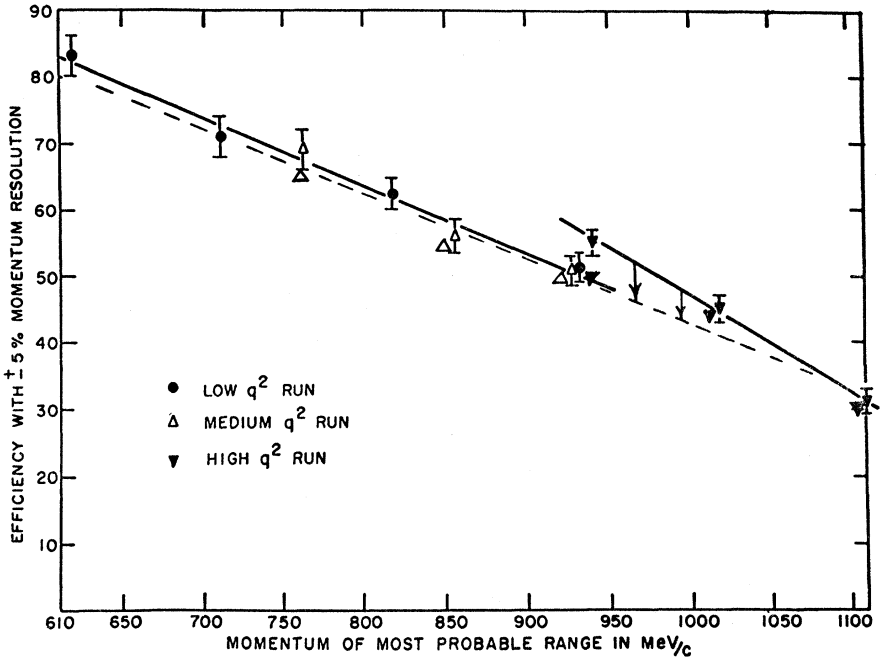

FIG. 4. The range beak efficiency (within ±5%), as obtained from the range calibration experiment. The effect of eliminating all events involving scattering angles greater than 15° is shown by the arrows.

elastic scattering yield when sections of the absorber were removed. The results of such measurements are discussed in detail in Appendix II and show that our elastic events contain less than 3% of π-p scatters.

The light concrete pion filter was poured into 32 ft of a 46-ft steel collimator having an inside diameter of 12 in., made from sections of a surplus naval cannon. These sections were then cast into heavy concrete in the form of standard 6 by 6 by 4-ft shielding blocks. Inserted into the last 6 ft of the collimator was a threshold gas Čerenkov counter, whose threshold was set for 1-BeV/c muons[17] (hence $\sim$1.35 BeV/c for pions). Eight feet of absorber were placed before quadrupoles M13 and M14 (see Fig. 2) and the remaining 24 ft immediately after. There followed an empty space and then 16 ft of collimator (*without* absorber).[18] The effect of this arrangement was to provide a high degree of collimation for the incident muons such that the overall angular divergence did not exceed 1° [see Figs. 5(a) and (b)]. Furthermore, in the region of the target a correlation between the transverse position of a beam track and its mean divergence was established as shown in Fig. 5(b). The beam appeared to have an effective source point, located approximately 380-in. upstream from the end of the last collimator.

The beam had a flux of 10^6 muons into a 10 by 10-in. area, per 10^{11} protons circulating in the AGS at full energy. The momentum spectrum extended from 1.0 to 6.5 BeV/c peaked at 2.5 BeV/c as indicated in Fig. 5(c).

[17] In view of the poor geometry of the beam and of the presence of knock-on electrons this threshold was not particularly sharp.

[18] For the low-momentum run (run A) the filter absorber arrangement was slightly different. The 8 ft of absorber shown before M13 and M14 were located in the free space before the collimators.

B. Detectors

The basic detection scheme can be best discussed with the aid of Fig. 3. The liquid-hydrogen target was of cylindrical shape 6 ft long and 18 in. in diameter. Optical spark chambers were used to record the recoil proton angle, the recoil proton range, and the angle of the scattered muon. The direction or energy of the incident muon was not measured (but was known to within the limits discussed in Sec. IIIA above).

The experiment was performed in three stages, each of which was made sensitive to elastic scattering for a different range of momentum transfers by placing additional absorbers in the path of the recoil proton before it entered the range chamber. The q^2 limits for each of these runs are indicated below:

Run A	$10<q^2<22$ F^{-2}	No absorber,
Run B	$13<q^2<23$ F^{-2}	2 in. of Al,
Run C	$19<q^2<31$ F^{-2}	2 in. of Al and 2 in. of Pb.

Furthermore, during run A the spark chambers were located closer to the target than in runs B and C to accept smaller scattering angles; and a lower incident beam rate was used. (Note that the setup in Fig. 3 refers to runs B and C.)

1. Triggering Counters and Logic

A trigger was obtained from a coincidence (time resolution $\sim$15 nsec) between (a) a beam pulse, (b) a recoil proton pulse, and (c) a scattered muon pulse. The beam pulse was defined by the Čerenkov counter (C), and a 10 by 10-in. beam counter (S) placed in front of the target. An array of anticoincidence counters (A) surrounded S; the anticoincidence consisted of six 12 by 36 by 1-in. scintillators placed mainly to protect

the proton counters. The beam counter was composed of five 2 by 10 by $\frac{1}{2}$-in. scintillator strips in order to reduce scaling losses[19]; such losses are important since the beam count determines the absolute normalization of our data. On the other hand inefficiencies in any of these counters have (to first order) no effect on our data.

The recoil protons were detected in two arrays of scintillators placed parallel to the beam axis, one before the angle chamber (Q counters) and one between the angle and range chamber (P counters), as shown in Fig. 3. The Q array consisted of 8 counters 12 by 24 by $\frac{1}{2}$ in.[20]; they were mounted one next to the other covering a total area of 96 by 24 in. The P array consisted of 20 counters 12 by 48 by $\frac{1}{2}$ in. placed at an angle of 30° with the beam axis so that each proton would traverse at least two adjacent counters. A P signal required a coincidence of any two adjacent P counters.

The logic that combined the P and Q signals was such that a count in Q_1 or Q_2 was put in coincidence only with P_1 through P_8; in Q_3 or Q_4 only with P_5 through P_{12}, etc. Thus, the proton tracks were required to be at an angle φ between 40° and 80° with respect to the beam axis, and consequently the number of spurious triggers was significantly reduced. The efficiency of the P and Q counters directly enters our results and therefore was carefully determined. The efficiency of the combined $\Sigma(PQ)$ signal was found to be 0.97 ± 0.02 (for runs B and C).

The scattered muons were detected in an array of three liquid scintillator counters (R) placed behind the 4-ft absorber. The scintillation tanks were of dimension 60 by 60 by 18 in. and were each filled with 1060 liters of liquid scintillator.[21] Each tank was viewed by 24 RCA 6655A photomultipliers placed to give a uniform signal, over the area of the tank, proportional to the energy loss of the muon and with minimal time jitter. Additional scintillators were used to protect the gaps between the tanks and for counting muons scattered at the smallest angles[22] [see Fig. 3(b)]. A muon traversing the liquid scintillator would loose ~100 MeV of energy making it possible to discriminate with ease against slow neutrons incident on the counters. The efficiency of the R counters also affects our data directly, and was measured to be better than 99%.

The fast logic was performed mainly with "nanocard" circuits.[23] Checks were built into the system so as to monitor the efficiency during the run, and several rates were continuously scaled and recorded. The circuits that triggered the chambers, and the slow logic were

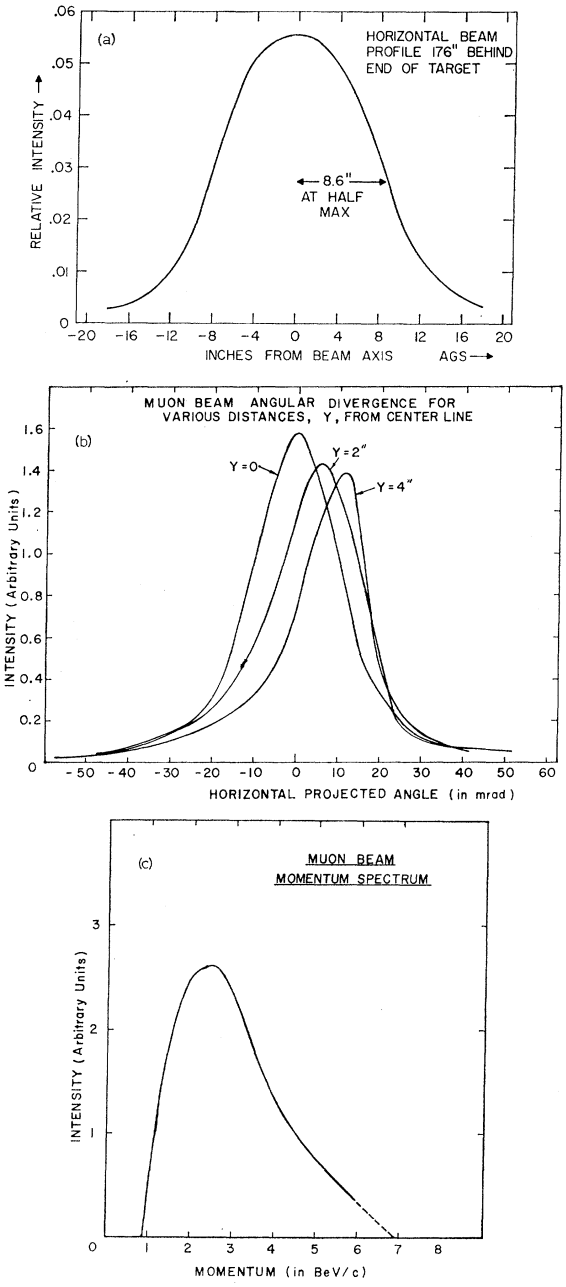

FIG. 5. Muon beam profiles. (a) Horizontal profile of the muon beam. The profile was taken 26-ft downstream from the end of the collimator. Allowing for the size of the beam, this corresponds to an over-all angular width of about 1°. (b) Angular correlation of the muon beam. The labeled y positions are those of the hodoscope counters S_i (see text, Sec. IIC1). The beam appears to come from a source subtending an angle of $\sim\frac{3}{4}°$ and located ~380-in. upstream from the end of the collimator. (c) Muon beam momentum spectrum. The lower limit corresponds to the threshold of the gas Čerenkov counter.

[19] 100-Mc/sec prescalers were used and the beam flux was taken as $\sum_{i=1}^{5} S_i\bar{C}\bar{A}$, (see Figs. 2 and 3). The *average rate* in S was of the order of 10 Mc/sec for runs B and C. For run A, where the rate was lower, a simple 10 by 10 by $\frac{1}{2}$-in. S counter was used.

[20] During run A the Q counters were only $\frac{1}{4}$ in. thick.

[21] Manufactured by Arapahoe Chemical Co., Boulder, Colo. Type HF.

[22] During run A the scintillator tanks were moved closer to the beam. This resulted in the primary beam crossing a section of the tank. This section was appropriately masked so that it was not viewed by the photomultipliers.

[23] R. Sugarman, F. C. Merritt, and W. A. Higinbotham, Brookhaven National Laboratory Report No. BNL 711 (T-248), 1962 (unpublished).

specially designed,[24] their functions being described in the next section.

2. *Spark Chambers*

(a) The proton angle chamber was made of thin Al plates ($\frac{1}{16}$ in.) in order to minimize multiple scattering. The active volume of the chamber was 114 in. long, 32 in. high, and 8 in. deep. It contained 95 plates assembled in modules of 5 with a $\frac{1}{2}$-in. gap. The plates were tilted so that their normal was at 60° to the beam axis (the plates had the same orientation as the P counters). The total material presented by the angle chamber into the path of the recoil protons, was on the average 7.5 g/cm^2. The chamber was photographed through its top window in 15° stereo by a single 70-mm camera.

(b) The proton range chamber consisted of 111 aluminum plates $\frac{3}{8}$ in. thick with $\frac{3}{8}$-in. gaps. The active volume was 144 in. long, 45.5 in. high, and 23 in. deep. Again, the plates were tilted with their normal at 60° to the beam axis and a track entering the chamber normal to the plates could traverse approximately 40 gaps before exiting. The chamber was photographed in one view only by a separate 70-mm camera. Both for the angle chamber and the range chamber, sets of prisms were used so as to permit observation of the entire depth of each gap. A count of the number of gaps traversed in combination with the angle chamber trajectory, yielded the range of the proton and hence its kinetic energy as discussed in Sec. II. The limits for a 60° proton in the range chamber were as follows: Run A, $180<T<450$ MeV; Run B, $230<T<485$ MeV; Run C, $360<T<580$ MeV; the difference being due to the absorber placed in front of the range chamber. Since the efficiency of the range chamber (especially at the end of a track) could affect the accuracy of the range determination, it was frequently checked by recording stray beam tracks.[25]

(c) The muon chambers were two identical assemblies of nine Al plates 4 by 4 ft by 1 in. thick separated by $\frac{3}{8}$-in. gaps. Lucite frames were used to space the plates and contain the gas.[26] Each was photographed in 18° stereo by a separate 70-mm camera.

All chambers were first flushed with helium and then filled with neon-helium[27] held at a slight overpressure (0.25 in. of water column). The spark-chamber trigger sequence was controlled by a set of logic circuits especially designed for the experiment.[24] All chambers were run at 15 kV and were fired simultaneously from a master spark gap which triggered 16 slave spark gaps attached directly to the chambers. Prior to firing the master spark gap, the control unit gated off all detection and scaling circuits to prevent spurious counts caused by spark-generated noise. These circuits were held off for the duration of the AGS pulse in which the trigger occurred. In view of the low triggering rate, this did not affect the duty cycle significantly. Attached to each chamber was an electroluminescent panel for recording the event number,[24] a set of fiducial lights for locating the track, and a floodlight for chamber illumination. After firing the chambers, the control unit activated each of these units and advanced the film.

IV. ANALYSIS OF THE DATA

As discussed before, three different runs were made; some relevant data are shown in Table IV(a). In addition, runs were taken with empty target, and with sections of the filter removed in order to measure the level of pion contamination (see Appendix II).

A. Scanning and Measuring

Since the triggering requirement was purposely quite loose, many of the frames could be rejected by the imposition of simple scanning criteria. These were as follows:

(1) A recoil proton track with 3 or more gaps must appear in the range chamber;
(2) the proton track must have an angle $>35°$ in both angle and range chamber;
(3) there must be at least one muon track; and
(4) if the proton interacted, the event was rejected except for scatters of $<5°$ in the angle chamber and $<15°$ in the range chamber.

To determine the scanning efficiency, a second scan was performed on parts of the film and newly selected candidates were processed to test for additional elastic events. The resulting scanning efficiency was found to be better than 99% in all cases.

The photographs of elastic scattering candidates were measured on Vanguard film-plane digitizers having a least count of 2.5 μ on film. This machine unit corresponded to 0.007 in. and 0.005 in. in the fiducial planes of the proton angle chamber and the muon chambers, respectively. The actual measurement resolution was approximately 0.020 in. in the fiducial planes in both cases because of spark image size. Results of the measurements were recorded on punched cars and were subsequently transferred to magnetic tape for reconstruction.

B. Reconstruction and Analysis

Optical transformations of the measured stereo track coordinates yielded the trajectories in space of the scattered muon and the recoil proton. We define the

[24] M. J. Tannenbaum, Brookhaven National Laboratory Report No. BNL 7033 (unpublished).
[25] By appropriate change of the PQ triggering requirement it was possible to photograph tracks that made an angle of 20° to 30° with the beam axis and traversed a major portion of the chamber.
[26] These chambers had been previously used in the Columbia-BNL neutrino experiment, G. Danby *et al.*, Phys. Rev. Letters **9**, 36 (1962).
[27] The usual 88% neon, 10% helium, 2% argon mixture.

x direction to be that of the beam axis, the z direction to be vertical, and the y direction to be horizontal toward the proton angle chamber. The origin is defined to be the center of the hydrogen target. The horizontal coordinates of the interaction vertex in the hydrogen were defined to be those of the intersection of the muon and proton trajectories projected on the xy plane. The z coordinate of the interaction vertex was taken midway between the scattering and recoil trajectories at their xy crossing point. The incident trajectory was *defined* by the interaction vertex and the apparent source point of the beam (−455 in.,0,0) mentioned in Sec. IIIB1. The vertex was required to lie within a defined fiducial volume (inside the hydrogen target).

Associated with the scattering vertex is a "vertex parameter" denoted by ΔZ, the vertical separation of the scattered and recoil trajectories at their xy-crossing point. Large values of ΔZ indicated a spurious combination of scattered and recoil trajectories. Since for most frames the muon chambers contained more than one track (due to spray from the beam halo), ΔZ provided a useful criterion for selecting the appropriate muon track.

From the reconstructed tracks we then computed the following quantities:

(a) The "coplanarity" angle ψ defined as

$$\psi=\cos^{-1}\left(\frac{\mathbf{p}_\mu}{|\mathbf{p}_\mu|}\cdot\frac{(\mathbf{P}_R\times\mathbf{k})}{|\mathbf{P}_R\times\mathbf{k}|}\right)-\tfrac{1}{2}\pi.$$

(b) The momentum of the incident muon under the assumption that the scattering was elastic. For inelastic events the momentum so computed was found to be much higher than 6 BeV/c providing a powerful criterion for their rejection.[28]

(c) The momentum of the recoil proton P_c, as calculated from the scattering angles under the assumption of elastic scattering. If we also assume that the proton reached the end of its range in the proton range chamber we can compute its observed momentum P_0. The range-energy relation used was fit to Sternheimer's formula[29] as explained in more detail in Appendix III. We define an "elasticity" parameter $Dp=(P_c-P_0)/P_0$, which is a measure of the goodness of fit to a two-body elastic scattering event. We mention again that $Dp\neq 0$ arises *either* because of incorrect P_c (that is, the event was not elastic), or through incorrect P_0 (that is, the proton did not reach the end of its range), or when both P_c and P_0 are incorrect.

(d) The momentum transfer (q^2) for an elastic event as obtained from the *observed* range of the recoil proton.

By an empirical study of the distributions mentioned above one can decide on selection criteria to be imposed on each distribution; at the same time one must estimate the loss of true events due to these criteria as well as the level of background events that are included. Such a study was done systematically by varying one selection criterion while others were held fixed and resulted in the adoption of the limits given in Table II (see also Figs. 6, 7, and 8).

TABLE II. Selection criteria for elastic events.

(a) Run A data				
(1)	-32	$\leq x_{\text{int}}\leq+32$	in.	(interaction x coordinate)
(2)	0	$\leq R_{\text{int}}\leq$ 9	in.	(interaction radius)
(3)	1.5	$\leq k\leq$ 6.0	BeV/c	(computed incident momentum)
(4)	-3.5	$\leq\Delta Z\leq+4.5$	in.	(vertical separation of tracks see text for definition)
(5)	-2.0	$\leq\psi\leq$ 3.2	deg	(coplanarity; see text)
(6)	-0.08	$\leq Dp\leq+0.22$		(elasticity $(p_c-p_0)/p_0$; see text)
(7)	-10	$\leq Dx'\leq+10$	in.	(transverse separation between end of angle chamber track and beginning of range chamber track)
(8)	The projected angle chamber trajectory must pass through the rear wall of the range chamber.			
(9)	At least 3 sparks and 4 gaps traversed in the range chamber (required at the scanning stage).			
(10)	At least 3 empty gaps in the range chamber between the end of the track and the back of the chamber.			
(11)	Proton interactions restricted by scanning criteria.			
(b) Differences corresponding to runs B and C				
(4′)		$-4\leq\Delta Z\leq+6$	in.	
(6′)		$-0.095\leq Dp\leq+0.165$	(run B)	
		$-0.10\leq Dp\leq+0.10$	(run C)	

A serious inefficiency occurs in the determination of the true observed range. Figure 4 shows the probability that a proton of given momentum will reach the end of its range. These data were obtained from a separate "calibration run" discussed in detail in Appendix III, and are in agreement with the known proton-nucleus cross sections.

A computer simulation of the entire scattering experiment using Monte Carlo techniques[30,31] was undertaken to include accurately in the experimental results the over-all detection efficiency for the experiment, including solid angle, multiple scattering, ionization loss, range straggling, nuclear interactions, measurement resolution, and all selection criteria. The nuclear-interaction model constructed for the program used the known data for proton-nucleon and proton-nucleus elastic and inelastic scattering; it required two fitted parameters which were determined in a successful simulation of the range calibration experiment.[30]

Measurement resolution was included in the Monte Carlo data by subjecting the trajectories of generated events to a stereo "measurement" which included an

[28] For elastic scatters the laboratory angle between the scattered muon and recoil proton ($\varphi+\theta$) gives a close estimate of the incident momentum k. This is not very sensitive to the exact direction of $\mathbf{k}$.

[29] R. M. Sternheimer, Phys. Rev. **115**, 137 (1959).

[30] M. J. Tannenbaum, thesis, Columbia University, 1965 (unpublished).

[31] S. Bender, S. Kaplan, and M. Tannenbaum, Brookhaven National Laboratory Report BNL 10166, AMD405, 1966 (unpublished).

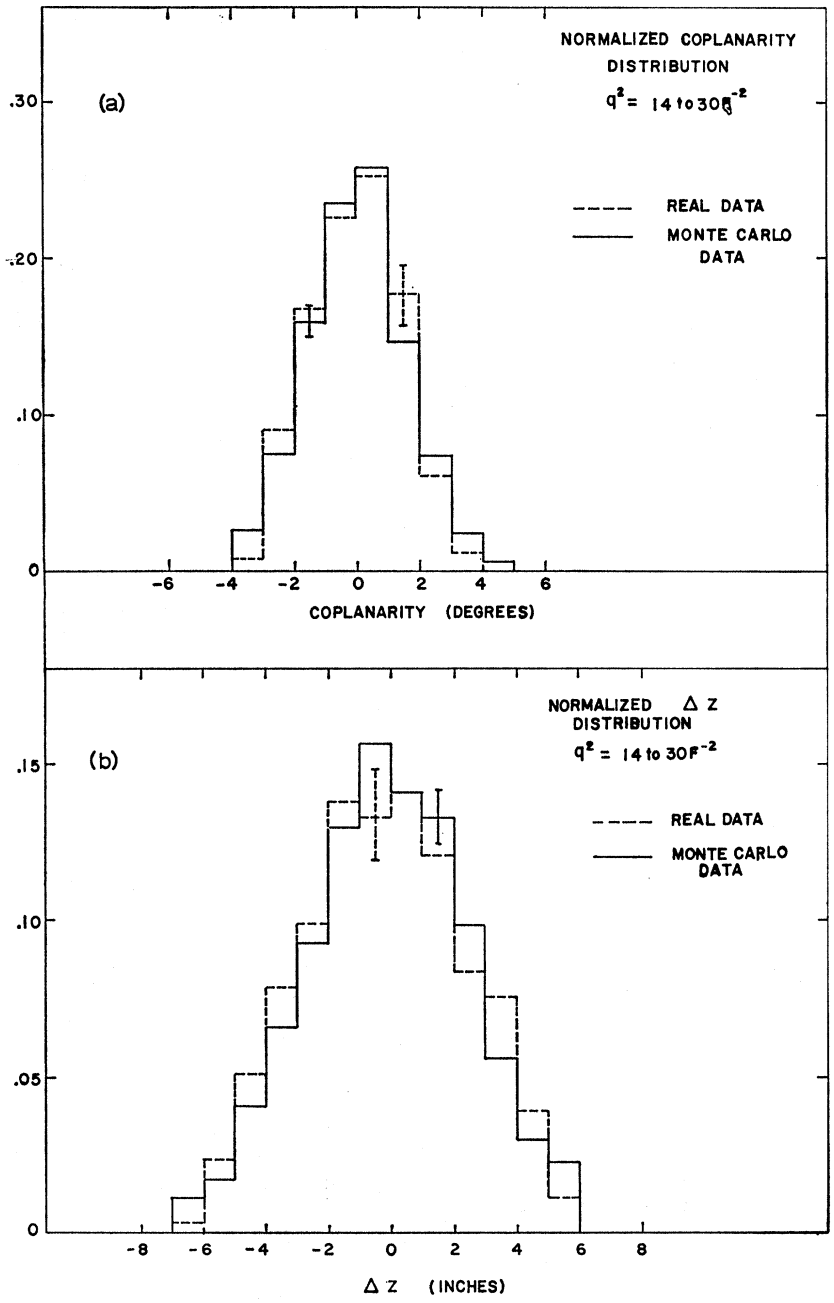

FIG. 6. (a) Distribution in ΔZ for selected events for runs B and C. The arrows indicate final selection limits for these runs. (b) Distribution in coplanarity angle (ψ) for selected events for runs B and C. The Monte Carlo program is discussed in the text.

error generated according to a normal distribution with an assumed variance. These "measurements" were then reconstructed and selected by the same procedure as were the real data. This process was repeated with a different variance until the Monte Carlo distributions in ΔZ and the coplanarity angle agreed in width with those of the real data. Comparison of the Monte Carlo distributions with the experimental distributions in ΔZ and coplanarity for runs B and C are shown in Figs. 6(a) and (b).

A comparison of the "elasticity" distribution (Dp) for real and Monte Carlo events is shown in Figs. 7(a) and (b) for runs A and C, respectively. The existence of a peak centered around $Dp=0$ confirms that two-body elastic scatters are observed, and it gives a measure of the background. For both the real data and the Monte Carlo data, a tail at higher values of Dp can be seen, corresponding to nuclear absorption of recoil protons. The distributions for the real data show an additional flat background of inelastic and accidental events. Comparison of the real distributions with the Monte Carlo distributions showed that the background included in the elastic sample was 6% for runs A and C and 3% for run B.

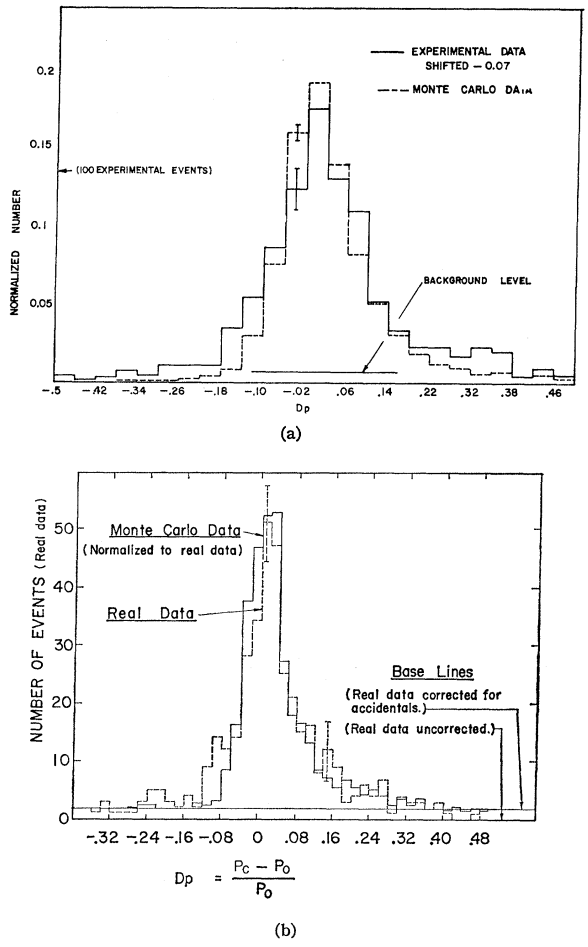

FIG. 7. Distribution in recoil momentum correlation (Dp) for selected events. (a) For run A. (b) For run C.

From Table II (entries 6 and 6′) and from Fig. 7(a) one notes that an asymmetry appears in the position of the Dp peak, especially for the run-A data.[32] A careful review of the recoil proton range measurement confirmed that this is not the cause of the shifts in Dp; we believe that these shifts reflect minor systematic errors in the reconstruction geometry.

A comparison of the measured beam momentum spectrum with the distribution in the reconstructed incident momentum k calculated from two-body elastic scattering kinematics is shown in Fig. 8 for run A. Allowance must be made for the acceptance of the detection apparatus; nevertheless, the agreement is quite good. Because the limits imposed on k ($1.5<k<6.0$ BeV/c) are narrower than the beam momentum spread, only 0.90 ± 0.02 of the recorded incident flux can contribute acceptable events.

In summary, the Monte Carlo calculation which is essential in the comparison of data and hypothesis is tested and constrained in many different situations.

[32] A similar but smaller effect appears also in entries (4) and (5) of Table II.

C. Systematic Effects

The q^2-independent corrections applied to the data were (i) scanning efficiency, (ii) counter efficiency for P, Q, and R counters, (iii) flux corrections, (iv) target wall scattering, (v) pion scattering contamination, (vi) contamination by inelastic scattering and accidental events (background), and (vii) radiative corrections. In Table III are listed the magnitudes of these effects and the associated systematic errors as we understand them.

The flux corrections for all three runs took account of (1) accidental CS coincidences, (2) dead-time losses in the electronics, (3) the recording of a knock-on electron in one beam channel simultaneous with a triggering muon in another channel (runs B and C only), (4) that portion of accidental CS coincidences corresponding to acceptable muons missed because of Čerenkov-counter inefficiency, and (5) the flux lying outside the range $1.5<k<6.0$ BeV/c.

A rather loose set of selection criteria imposed on our empty-target data yielded no acceptable events, indicating that target wall scattering is completely negligible.

The analysis of the pion contamination data is discussed in detail in Appendix II. It indicates that even under the most conservative considerations, pion scatters in our elastic sample are $<3\%$. This result is obtained by assuming that the pion contamination is completely dominated by regeneration in the filter; it corresponds to an effective π/μ ratio at the hydrogen target of $<3\times10^{-6}$.

The background events (inelastic and accidentals) were obtained, as explained in the previous section, from the "elasticity" distribution. An independent estimate of accidental event contamination was obtained by forming combinations of unrelated muon and proton tracks and testing the resulting sample for elastic events. The results indicated an accidental contamination of $(7.9\pm2.5)\%$ for run A and an upper limit of

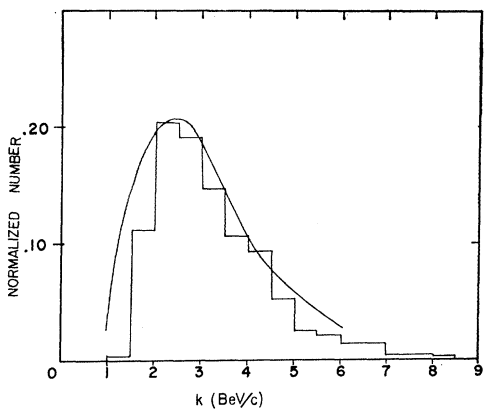

FIG. 8. Distribution in reconstructed incident momentum (k) for selected events for run A. The limits on k have been relaxed. The measured spectrum (solid line) is shown for comparison.

TABLE III. Systematic effects (values given are factors by which the observed yield was affected).

	Effect	Run A	Run B	Run C
(i)	Scanning efficiency	0.99 ±0.01	0.99 ±0.01	0.99 ±0.01
(ii)	Counter efficiency	0.95 ±0.02	0.97 ±0.02	0.97 ±0.02
(iii)	Flux loss from incident momentum selection	0.90 ±0.02	Same	Same
	Flux counting error	1.01 ±0.01	0.92 ±0.03	0.92 ±0.03
(iv)	Target wall scattering	1.00	Same	Same
(v)	Pion scattering contamination	$1.0_{-0,00}^{+0.03}$	Same	Same
(vi)	Background contamination	1.06 ±0.01	1.03 ±0.01	1.06 ±0.01
(vii)	Radiative corrections	0.989±0.006	0.977±0.003	0.977±0.003
(viii)	Measuring and processing efficiency	0.98 ±0.02	0.96 ±0.02	0.98 ±0.02
	Total	0.88 ±0.05	0.77 ±0.05	0.81 ±0.05

7% for runs B and C, in agreement with the direct result.

The radiative corrections to the Rosenbluth formula were calculated for the geometry of this experiment by Moran.[33] Integration over the final-state variables corresponded to the selection limits imposed for elastic scattering events, with the result that hard-photon emission was confined to directions parallel to either the incident muon or the scattered muon. Most events in the latter case fail the muon trigger requirements. The correction applied to runs B and C was (2.3±0.3)% and for run A (1.1±0.6)%, and was insensitive to q^2.

V. RESULTS AND INTERPRETATION

Our results are summarized in Table IV. In Table IV(a) we indicate for each interval of q^2 the observed yield of elastic events and the corresponding corrected muon flux. The systematic effects listed in Table III have been taken into account by correcting the counted flux accordingly.

We used the Monte Carlo program, described previously, to calculate the expected yield of elastic events according to the Rosenbluth formula using electron-proton form factors.[34] The yield so calculated is shown in Column 3 of Table IV(a).

In the last column of Table IV(a) we give the measured μ-p elastic scattering cross section integrated over each bin. This is obtained from

$$\Delta\sigma_{\mu p}=\frac{\text{Experimental yield in interval of } q^2}{\text{Monte Carlo expected yield in same interval}}\Delta\sigma_{ep},$$

where $\Delta\sigma_{ep}$ is the integral (over the q^2 limits) of the electron-proton cross section used in the Monte Carlo calculation. The indicated error is only statistical due to both the experimental and Monte Carlo yields. Note that in Table IV(a) the equivalent Monte Carlo flux is not the same as the flux obtained during the experiment; thus the figures of Column 3 must be appropriately scaled.

In Table IV(b) we give the measured differential cross section $d\sigma/dq^2$ for muon-proton elastic scattering evaluated at the center of each bin.[35] These results are also shown in Fig. 9; here the vertical bars indicate the statistical error and the horizontal bars the size of the

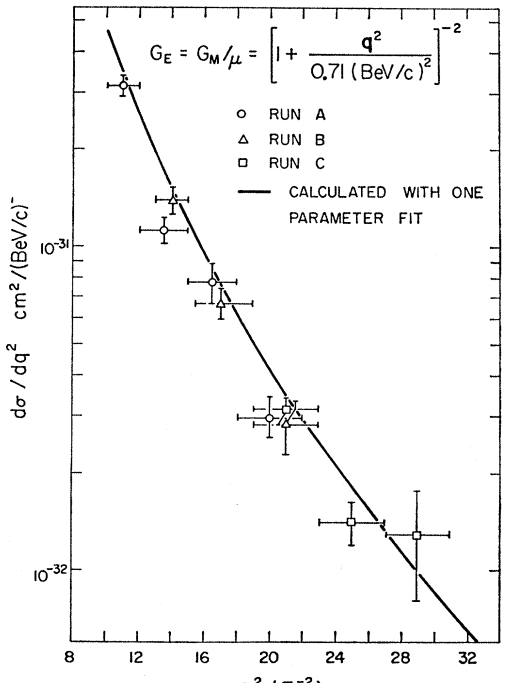

FIG. 9. Plot of the experimentally measured muon-proton elastic scattering cross section $d\sigma/dq^2$. The solid line is the prediction of the one-parameter fit to the electron-proton data (Ref. 36). Horizontal bars indicate the acceptance width of each q^2 interval. Vertical bars represent statistical errors only.

[33] W. P. Moran (private communication). The calculation was based on the work of Y. S. Tsai [Phys. Rev. **122**, 1898 (1961)] using the technique of D. R. Yennie, S. C. Frautchi, and H. Suura [Ann. Phys. (N.Y.) **13**, 379 (1961)] to extract and cancel the infrared divergences. The noninfrared portions of the two-photon exchange terms and the proton-vertex modification term were neglected as was the proton bremsstrahlung term. The interference term between muon bremsstrahlung and proton bremsstrahlung was retained.

[34] For run A the form factors were taken from the (b') fit of C. de Vries, R. Hofstadter, A. Johansson, and R. Herman, Phys. Rev. **134**, B848 (1964). For runs B and C a one-parameter form factor was used as given by L. N. Hand, D. G. Miller, and R. Wilson, Rev. Mod. Phys. **35**, 335 (1963).

[35] A calculation of $d\sigma/dq^2$ using directly the solid angle and nuclear-interaction efficiency and flux was also made (without the Monte Carlo program); as expected these results are in agreement with the more sophisticated approach described in the text.

TABLE IV. Summary of results.

(a) Experimental results on muon-proton elastic scattering

q^2 interval (F^{-2})	Yield (experimental)	Yield (Monte Carlo)	$\Delta\sigma_{\mu p}$ in q^2 interval (10^{-33} cm^2)
Run A			
10–12	253	514	25.0 ±1.9
12–15	148	441	13.5 +1.3
15–18	74	163	9.3 ±1.3
18–22	47	139	4.74±0.81
Corrected flux	2.514×10^{10}	4.809×10^{10}	
Total number of frames	30 000		
Frames accepted for measurement	6000		
Run B			
13–15	123	403	10.97±1.1
15–19	111	384	10.81±1.2
19–23	35	132	4.50±0.85
Corrected flux	6.267×10^{10}	18.05×10^{10}	
Total number of frames	27 000		
Frames accepted for measurement	3000		
Run C			
19–23	153	522	5.03±0.46
23–27	56	216	2.24±0.34
27–31	10	23	2.05±0.78
Corrected flux	20.69×10^{10}	60.29×10^{10}	
Total number of frames	50 000		
Frames accepted for measurement	2000		

(b) Comparison of the experimental muon-proton elastic scattering cross section with the one-parameter fit to the electron-proton data[a,b] $G^2=G_E^2+(q^2/4M^2)G_M^2$ [see Eq. (2) in text].

q^2 (F^{-2})	$d\sigma/dq^2$ (experiment) [μb/(BeV/c)^2]	G^2 (experiment)	G^2 (one-parameter fit)[a]	$R=\frac{G^2(\text{experiment})}{G^2(\text{one-parameter})}$
Run A				
11	0.3160	0.271	0.294	0.921±0.07
13.5	0.1120	0.151	0.236	0.640±0.06
16.5	0.0778	0.164	0.184	0.894±0.13
20	0.0296	0.097	0.141	0.689±0.12
Run B				
14	0.1393	0.204	0.226	0.901±0.09
17	0.0669	0.151	0.177	0.856±0.09
21	0.0281	0.103	0.131	0.788±0.15
Run C				
21	0.0314	0.115	0.131	0.880±0.08
25	0.0141	0.0778	0.0997	0.780±0.12
29	0.0129	0.102	0.0776	1.312±0.50

[a] See Ref. 36.
[b] The errors on columns 2 and 3 are the same *percentage* errors corresponding to the absolute errors given in column 5.

q^2 bin from which the datum was obtained. The solid curve is the prediction of the one-parameter fit,[36] $G_E=G_M/\mu=(1+q^2/0.71)^{-2}$; q^2 in (BeV/c)^2.

In column 3 of Table IV(b) we give $G^2(q^2)$ [defined by Eq. (2)] as obtained from the measured values of $d\sigma/dq^2$. This is shown in Fig. 10, where again the solid line is the resulting value using the one-parameter fit, which is also given in column 4 of Table IV(b). Included in Fig. 10 are the values of $G^2(q^2)$ obtained from the electron-proton scattering data of Janssens *et al.*[37]

In the last column of Table IV(b) we give the ratio of our cross sections $d\sigma/dq^2$ to that predicted by the one-parameter fit[36] (that is, the ratio of column 3 to column 4). The error shown is the same percentage error as in column 4 of Table IV(a). The ratios so obtained are plotted in Fig. 11 as a function of q^2.

As is apparent from Figs. 10 and 11, the muon-proton scattering points seem to be lower than the corresponding electron-proton data. This can be due to absolute normalization errors (in either data), as discussed below. To obtain a more quantitative interpretation of our data we introduce a one-parameter lepton form factor $f(q^2)=1/(1+q^2/\Lambda^2)$, which multiplies the proton form factor.[14,38] The "cutoff" parameter Λ may be different for the muon and the electron. If we define a new parameter

$$\frac{1}{D^2}=\frac{1}{\Lambda_\mu^2}-\frac{1}{\Lambda_e^2}, \tag{3}$$

[36] L. H. Chan, K. W. Chen, J. R. Dunning, Jr., N. F. Ramsey, J. K. Walker, and R. Wilson, Phys. Rev. **141**, 1298 (1966).
[37] T. Janssens, R. Hofstadter, E. B. Hughes, and M. R. Yearian, Phys. Rev. **142**, 922 (1966).
[38] S. D. Drell, Ann. Phys. (N.Y.) **4**, 75 (1958); B. de Tollis, Nuovo Cimento **16**, 203 (1960); V. B. Berestetskii, O. N. Kroklin, and A. K. Khlebnikov, Zh. Eksperim. i Teor. Fiz. **30**, 788 (1956) [English transl.: Soviet Phys.—JETP **3**, 761 (1956)].

then to first order

$$R(q^2)=\frac{d\sigma_\mu}{dq^2}\Big/\frac{d\sigma_e}{dq^2}=\left(\frac{f_\mu}{f_e}\right)^2=\frac{1}{(1+q^2/D^2)^2}, \qquad (4)$$

and a comparison of the muon-proton and electron-proton elastic scattering cross section yields directly D^2.

In Fig. 11 the function $R(q^2)$ is shown for different values of D^2. The best fit is obtained for

$$D^{-2}=0.0067\ \mathrm{F}^2,$$

with a standard deviation of ± 0.0013 F^2; $\chi^2=17$ for 9 degrees of freedom.[39]

In order to take account of a discrepancy in the normalization, we show in Fig. 12 the best fit for D^{-2} as a function of N, where $(1-N)$ is a possible fractional discrepancy in the normalization of our experiment and of the electron data. The 95% confidence limits for D^{-2} are also indicated. We note that for $N=0.80$, $D^{-2}=0$.

To summarize our conclusions we give below the best value, and 95% confidence limit for D^2 both for $N=1$ and $N=0.80$.

Relative normalization N	Best fit D^{-2} (F^2)	95% confidence limit D^2 (F^{-2})	D (BeV/c)
1	0.0067 ± 0.0013	107	2.04
0.80	$0\ \pm0.0013$	308	3.5

It is therefore clear, that regardless of any possible small normalization errors the present experiment establishes at the 95% confidence level that if muon electron structural differences exist, they occur at a distance

$$D^{-1}<0.09\ \mathrm{F}.$$

Having thus established the main conclusion of this experiment we wish to make some brief comments on its relation to other experiments probing the electromagnetic properties of leptons.

(a) If the muon $g-2$ experiment is regarded as setting a limit on the muon-vertex function, then the recent measurements at CERN[7] provide a 95% confidence limit on $\Lambda_\mu^{-1}<0.18$ F. We may combine this limit with our limit on D^2 to arrive at an estimate for the electron parameter $\Lambda_e^{-2}=\Lambda_\mu^{-2}-D^{-2}$. Using $0<D^{-2}<0.0093$ F^2 we conclude that $\Lambda_e^{-1}<0.18$ F with 95% confidence. This is to be compared with the result of the colliding-beam experiment of Barber *et al.*,[10] which established $\Lambda_e^{-1}<0.26$ F (95% confidence).

(b) Alternatively, we may combine our limit $D^{-2}<0.0093$ F^2 with the limit of the colliding-beam experiments[10] to get a limit on the muon-vertex parameters: We get $\Lambda_\mu^{-1}<0.29$ F independently of any relation between the lepton-propagator modification and the lepton-vertex modifications that have been discussed by Drell and McClure[40] and by Kroll.[41]

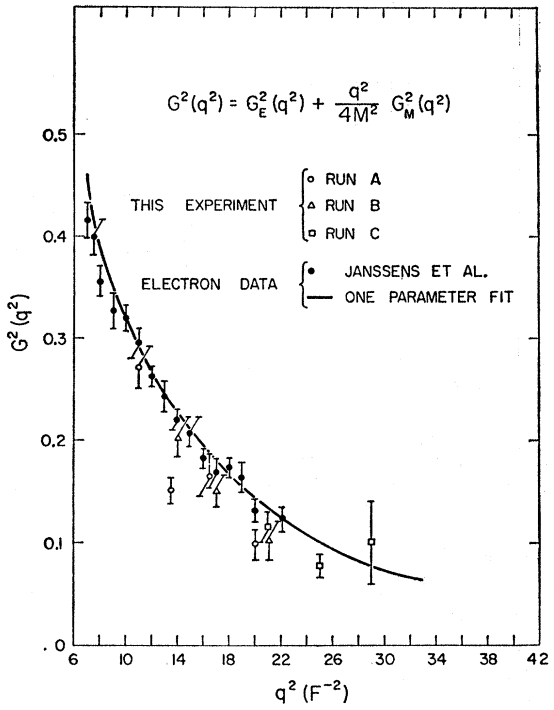

FIG. 10. The muon-proton form factor G^2 as obtained from this experiment. The solid line is the prediction of the one-parameter fit (Ref. 36). The values obtained for the electron-proton form factor by Janssens *et al.* (Ref. 37) are also shown. Systematic errors are not included.

ACKNOWLEDGMENTS

We are grateful to the many graduate assistants both at Columbia and Rochester who helped in several ways during the preparation, performance, and analysis of this experiment. We are also grateful for the unfailing support of the technical and engineering facilities of Brookhaven, Columbia, and Rochester, in particular to W. Hayes, J. Haufman, W. Murdock, and H. Schulman who assisted us during the run. Professor L. Marshall participated in the early stages of this experiment and was instrumental in the successful design of the muon transport system. Finally this experiment could not have been performed without the continuing support of the AGS staff and operating crews.

APPENDIX I: MEASUREMENT OF PION ATTENUATION IN LIGHT CONCRETE AND IRON AT 4.5, 6, AND 9 BeV/c

In the beam used for this experiment the desired purity of muons is obtained by passing the beam through sufficient absorber to eliminate the pions and

[39] Of the value $\chi^2=17$, the point at $q^2=12$–15 F^{-2} contributes 10.9. We have performed a fit excluding this point and find $D^{-2}=0.00462\pm0.00126$ F^2 with a χ^2 of 3.6 for eight degrees of freedom. This corresponds to $D>2.3$ BeV/c with a 95% confidence limit.

[40] J. A. McClure and S. D. Drell, Nuovo Cimento **37**, 1638 (1965).

[41] N. M. Kroll, Nuovo Cimento **45A**, 65 (1966).

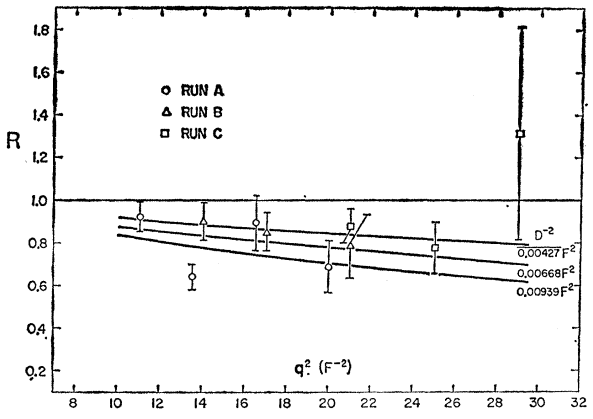

FIG. 11. Ratio of corrected experimental yield to normalized Monte Carlo yield obtained by using the one-parameter fit (Ref. 36). The curves represent the best-fit values and the 95% confidence levels for the fit of Eq. (4) to these data.

other strongly interacting particles. Therefore, a knowledge of the pion attenuation in the absorber material is essential; such data however were not available and we performed measurements at the energies indicated above. Here we give a brief discussion of this work, whereas more details can be found in an unpublished report by Tinlot.[42]

The measurements were performed at the Brookhaven AGS using a well collimated (1-in.-diameter), momentum-selected π^+ beam. A high-resolution differential Čerenkov counter permitted the separation of μ mesons so that the muon contamination varied from 1×10^{-3} at 4.5 BeV/c to $\sim10^{-2}$ at the highest momentum. The beam was made incident on a varying thickness of absorber and the transmission was measured by two large 18 by 18 by 2-in. counters placed behind the absorber. The counters were separated by 8 in. of lead so that both integral and differential transmission curves could be taken simultaneously. The latter ones are subject to fewer systematic errors and were used for extracting the absorption mean free path. Appropriate corrections for pion decay and accidental coincidences were applied. The large size of the counters minimized the effect of multiple scattering in the absorber.

The differential transmission curves exhibit the well-known "transition region" where more particles emerge from the absorber than were incident on it. This is due to the development of the nuclear cascade. Beyond the transition region the transmission decreases exponentially with absorber thickness; the coefficient of the exponent is the mean free path for absorption. The results obtained in this way are presented in Table V.

Finally, one may try to fit the experimental transmission curves by a model which takes into account the development of the nuclear cascade. Such a model however, requires a large number of input parameters;

TABLE V. Pion absorption lengths in light concrete and iron.

Momentum (BeV/c)	λ (ft) Concrete	Iron	λ (g/cm²) Concrete	Iron
4.5	1.6	0.68	118	155
6.0	1.65	0.68	121	155
9.0	1.75	0.78	129	179
Densities	Light concrete:		2.4 g/cm³	
	Iron:		7.83 g/cm³	

instead, we used a simple one-dimensional Monte Carlo calculation.[43] The results of this calculation are shown in Fig. 13 (solid curve) under the assumption that each primary pion produces three secondaries and that no tertiaries are produced; the interaction mean free paths for primaries and secondaries are set equal. Also in Fig. 13 is shown the experimentally obtained integral transmission curve for 6-BeV/c π mesons (dashed curve). The two curves are in satisfactory agreement and indicate that in the region studied the exponential decrease follows 1.2 α, where α is the interaction mean free path.

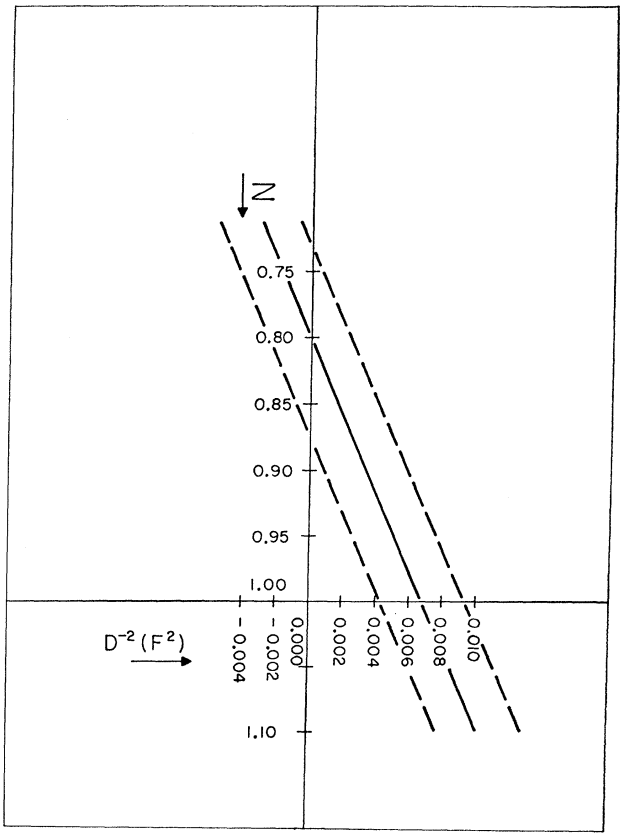

FIG. 12. Best-fit values of D^2 for different values of the normalization parameter N. The 95% confidence limits on D^2 are also indicated by the dashed curves.

[42] J. Tinlot, Brookhaven National Laboratory Report No. BNL 750 (T276), 1961 (unpublished).

[43] S. Thakore, A. C. Melissinos, and J. Tinlot, University of Rochester Report N.Y.O.-10132 (unpublished).

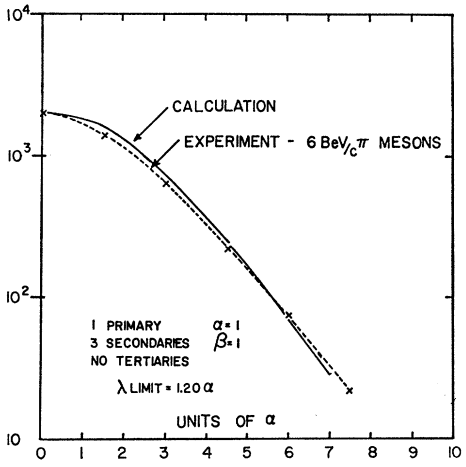

FIG. 13. Comparison of a cascade model with the 6-BeV attenuation data. α, β represent the interaction mean free paths of primary and secondary pions, respectively. The abscissa is distance in units of α, and the ordinate is a measure of relative intensity.

APPENDIX II: MEASUREMENT OF THE PION CONTAMINATION

In the previous Appendix it was shown how the mean free path for pion absorption was experimentally measured. This type of direct measurement however cannot be performed over the large attenuation (10^{-8}) introduced by the main-beam absorber (see Fig. 2). Furthermore, as discussed in the text, the muons, while traversing the absorber, electroproduce pions.[16] Such a contamination clearly will be in equilibrium with the muon flux and cannot be reduced by the further addition of absorber.[44] However, absorber placed after the hydrogen target does reduce the yield of any pion-proton elastic scatters by preventing the pions from reaching the R counters[45] (see Fig. 3).

If we use the data of Table V we find that the 32-ft light concrete filter provides an attenuation of 10^{-8} (19 mean free paths effective), whereas the 4-ft R absorber provides an additional factor $\frac{1}{12}$. These estimates neglect the equilibrium pion contribution.

We can, however, obtain a realistic estimate of the beam contamination by making use of the large pion-proton elastic scattering cross section.[15] Let α be the fraction of pions in the beam; then the yield of observed elastic events is

$$Y \propto \sigma_{\mu\text{-}p}+\alpha\sigma_{\pi\text{-}p}\simeq\sigma_{\mu\text{-}p}(1+\alpha\times 10^4).$$

We have performed scattering measurements with the R absorber removed and 7 ft of the main absorber removed. Let N be the increase in the pion contamination which results from such absorber removal; in this case the yield of scattering events must be

$$Y_c\simeq\sigma_{\mu\text{-}p}(1+N\alpha\times 10^4).$$

Thus the error in our observed yield is

$$\alpha\times 10^4=\frac{Y_c/Y-1}{N-Y_c/Y}.$$

The observed ratio of elastic yield is $Y_c/Y=1.34\pm0.28$, and it remains to estimate N. If we neglect the electroproduced pions, $N\sim840$ so that $\alpha\times10^4\sim(0.04\pm0.03)\%$, completely negligible, and in agreement with our estimate of $\alpha\sim10^{-8}$. On the other hand if we assume that the electroproduced pions have reached complete equilibrium after 25 ft of absorber, we must choose $N\sim12$. In that case the contribution of pions to our elastic scattering yield becomes $\alpha\times10^4\sim(3.2\pm2.8)\%$. This last number clearly is the *upper* limit which we can obtain under the most conservative estimate.

APPENDIX III: RANGE CALIBRATION EXPERIMENT

As discussed in the text the measurement of the recoil proton's energy by range introduces a large probability for nuclear interaction in the range chamber. Exact knowledge of this interaction probability is essential to the determination of the muon elastic

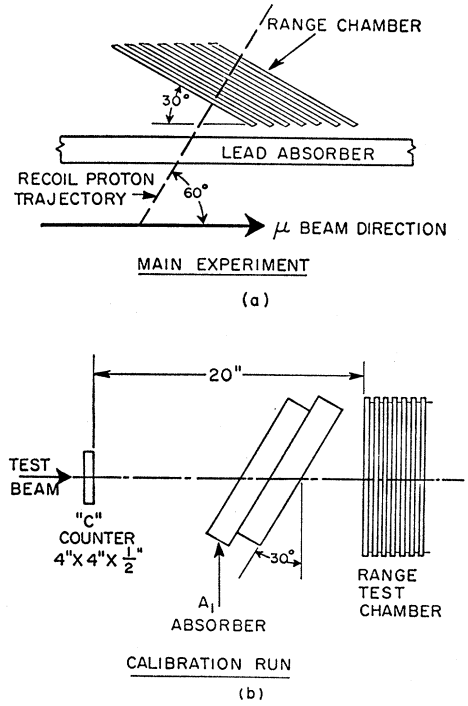

FIG. 14. Schematic comparison of the range calibration experiment with the proton range measurement of the main experiment.

[44] We have estimated the yield of electroproduced pions by a Weizsäcker-Williams-type calculation and find a π/μ ratio of the order of $\alpha\sim10^{-5}$. See also R. W. Ellsworth, University of Rochester, thesis, 1965 (unpublished), Appendix III.

[45] We note however that an increase of the R-absorber rejection (thickness) is not useful because of the probability of decay of pions into muons before entering the absorber. For our geometry and for the average momentum of 2 BeV/c this limit is at the 4% level.

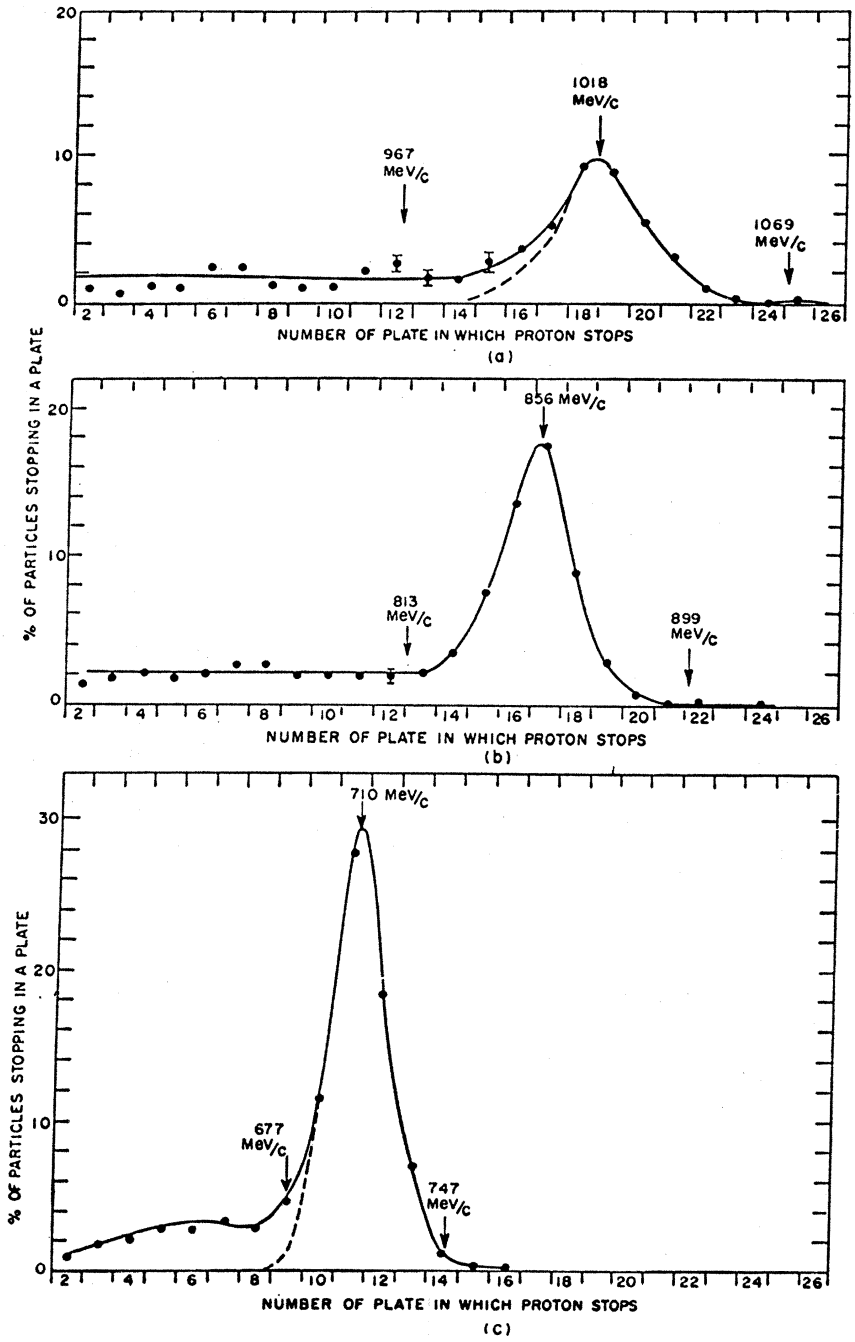

FIG. 15. Typical gap distributions from the range calibration experiment, for (a) high q^2 ($p_{\text{inc}}=1018$ MeV/c); (b) medium q^2 ($p_{\text{inc}}=856$ MeV/c); (c) low q^2 ($p_{\text{inc}}=710$ MeV/c).

scattering cross section. In addition, an accurate knowledge of the range-energy relation[29] under the special conditions of our experimental setup was deemed necessary.

For these reasons a control experiment was performed at the Brookhaven Cosmotron using a facsimile of the proton-range chamber. The test chamber was exposed to a well-defined ($\Delta p/p=\pm 2\%$) proton beam and appropriate absorbers were placed in front of it, the material being the same as in the three main experimental runs (A, B, and C). This experiment has been described in detail elsewhere[46]; a brief summary and the main conclusions are given below.

Protons were selected in a 20-ft time-of-flight counter telescope. The spark chamber was 12 by 12 in. square and contained 35, $\frac{3}{8}$-in. aluminum plates. The absorber was tilted at 30° as shown in Fig. 14(b) so as to simulate the mean direction of the recoil protons [see Figs. 14(a)

[46] R. Ellsworth, L. Lederman, and M. Tannenbaum, Nevis Cyclotron Laboratory Report No. R-417, 1964 (unpublished).

and 3(a)]. For each of the three absorber configurations, three momenta were studied and for each run approximately 1200 events were photographed.

The photographs for each run were processed to obtain the following distributions: (i) gaps traversed in the chamber, (ii) angle of scattering in the absorber, and (iii) angle of scattering in the chamber. In addition, the percentage of protons lost in the absorber and the percentage passing through the sides of the chamber were recorded.

Typical gap distributions are shown in Fig. 15; in addition to the range peak, a uniform distribution corresponding to nuclear absorption at ranges below those included in the range peak is evident. The width of the range peak shows, in all cases, that the resolution of the range measurement is equivalent to less than $\pm 5\%$ of the incident proton momentum. In Fig. 16 is plotted the most probable range in g/cm^2 of aluminum-equivalent[47] versus the incident proton momentum. For comparison, the theoretical predictions of Sternheimer[29] are plotted. The 2% discrepancy is attributed to a systematic error in the peak momentum value of the proton beam.[46]

From the data we also obtain the "range peak efficiency," which is defined as the fraction of incident protons reaching the range peak. It is more profitable however to plot the fraction of protons reaching a range corresponding to $\pm 5\%$ of their true range; this has been shown in Fig. 4 where the effects of nuclear absorption with increasing momentum are evident. The straight lines are visual fits to the data.

The data for the two higher q^2 runs (corresponding to runs B and C) were reprocessed with a limit of 15° imposed on the projected scattering angles. This limit altered the range efficiency for the high-q^2 run (run C) as shown by the arrows in Fig. 4. We conclude that nearly all of the proton scatterings by greater than 15° occurred in the 2-in. lead absorber.

The results of the calibration experiment verified that the recoil proton kinetic energies of the main experiment could be determined by using the results of

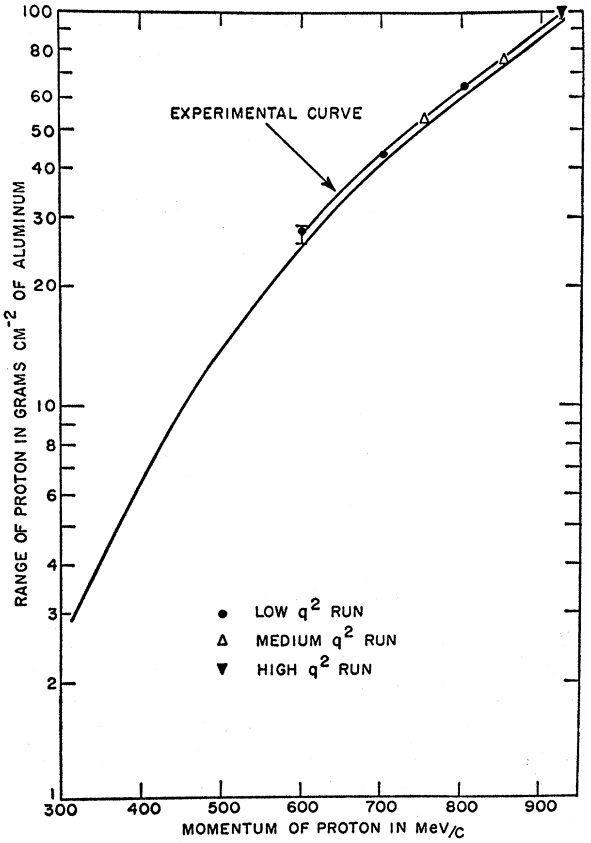

FIG. 16. Comparison of theoretical and measured range-momentum relations for protons in aluminum. The lower curve corresponds to the relation of Sternheimer (Ref. 29).

Sternheimer's range-energy calculations,[29] and further enabled a calculation of nuclear-interaction losses to the μ-p elastic scattering sample of the main experiment. A comprehensive computer simulation of the main experiment was made possible by fitting a one-parameter model for nuclear interactions of the recoil proton to the data of the range calibration experiment.[30] The one parameter is the fraction of inelastically scattered protons which lose sufficient energy so that they are effectively stopped by inelastic interactions; the rest of the inelastically interacting protons are assumed to scatter quasielastically. This parameter is taken to have different values for heavy (Pb) and light (Al) nuclei.

[47] All materials were converted to aluminum-equivalent by use of the relation (Range)$(dE/dx)_{\min}$ = (constant) which holds to 4% for carbon, aluminum, hydrogen, and lead for the recoil proton energies of this experiment.